

# Journal of Fire Sciences

<http://jfs.sagepub.com/>

---

## **Effects of Fuel Location and Distribution on Full-Scale Underventilated Compartment Fires**

Cheol-Hong Hwang, Andrew Lock, Matthew Bundy, Erik Johnsson and Gwon Hyun Ko

*Journal of Fire Sciences* 2011 29: 21 originally published online 24 May 2010

DOI: 10.1177/0734904110372119

The online version of this article can be found at:

<http://jfs.sagepub.com/content/29/1/21>

---

Published by:



<http://www.sagepublications.com>

**Additional services and information for *Journal of Fire Sciences* can be found at:**

**Email Alerts:** <http://jfs.sagepub.com/cgi/alerts>

**Subscriptions:** <http://jfs.sagepub.com/subscriptions>

**Reprints:** <http://www.sagepub.com/journalsReprints.nav>

**Permissions:** <http://www.sagepub.com/journalsPermissions.nav>

**Citations:** <http://jfs.sagepub.com/content/29/1/21.refs.html>

---

---

# Effects of Fuel Location and Distribution on Full-Scale Underventilated Compartment Fires

**CHEOL-HONG HWANG**

*Department of Fire and Disaster Prevention, Daejeon University, 96-3, Yongun-Dong, Dong-Gu, Daejeon 300-716, South Korea*

**ANDREW LOCK,\* MATTHEW BUNDY AND ERIK JOHNSON**

*Building and Fire Research Laboratory, National Institute of Standards and Technology, 100 Bureau Drive, Stop 8663, Gaithersburg, MD 20899-8663, USA*

**GWON HYUN KO**

*Department of Architecture and Fire Administration, Dongyang University, Punggi-Up, Yongju-Si, Gyeongsangbuk-Do 750-711, South Korea*

(Received March 6, 2010)

---

---

**ABSTRACT:** An experimental study was conducted to investigate the effects of fuel location and distribution on full-scale underventilated compartment fires in an ISO 9705 room. Heptane fuel was burned in three different fuel distributions: single centered burner (SCB), single rear burner (SRB), and two distributed burner (TDB). It was experimentally observed that variations in fuel placement did not significantly affect the global steady state underventilated fire characteristics such as fuel mass loss rate, heat release rate, combustion efficiency, global equivalence ratio, and global CO emission outside the compartment for these simple distributions. Supplemental numerical simulations reveal that the local characteristics of thermal and chemical environments depend on the fuel placement between the front and rear region inside the compartment. At the front region, the local fire characteristics were nearly the

---

\*Author to whom correspondence should be addressed. E-mail: [andrew.lock@nist.gov](mailto:andrew.lock@nist.gov)  
Figures 1–13 appear in color online: <http://jfs.sagepub.com>

JOURNAL OF FIRE SCIENCES, VOL. 29 – January 2011

21

0734-9041/11/01 0021–32 \$10.00/0 DOI: 10.1177/0734904110372119

© The Author(s), 2011. Reprints and permissions:  
<http://www.sagepub.co.uk/journalsPermissions.nav>

same regardless of fuel placement. Changes in fuel location and distribution resulted in changes in temperature, total heat flux, CO<sub>2</sub>, and CO volume fraction at the rear region. Burner placement led to changes in the mixture fraction, flow dynamics, and variations in CO production in the back of the compartment.

**KEY WORDS:** compartment fire, underventilated fire, fuel distribution, ISO 9705 room, heptane.

## INTRODUCTION

FIRE BEHAVIOR, INCLUDING chemical kinetics, heat transfer, fluid dynamics, turbulence, and material properties, is one of the most complex phenomena considered in combustion science [1]. In particular, compartment fires can occur with a variety of configurations [2], fuel types [3], fuel distributions [4], and ventilation conditions [5]. The current study is part of a larger project aimed at better understanding underventilated compartment fire dynamics to facilitate model development [6,7]. This article presents findings related to the effects of fuel location and distribution on the global structure of full-scale underventilated compartment fires.

Most research has been focused on a fire generated in a geometrically centered burner inside a compartment [8–10]. However, it is not well understood how the location and distribution of the available fuel materials may affect the fire growth, toxic product generation, and time to flashover as well as the internal flow dynamics and thermal environment within a compartment. Tran [11] carried out experiments of bench-scale and full-scale compartment fires with different burner locations to validate and develop a wall fire model in overventilated fire conditions. He found that there were significant changes in heat release rate (HRR) and time to flashover when the burner was located at either the centerline of the rear wall or the rear corner. Snegirev et al. [12] changed the distance between the burner and doorway to investigate the dimensionless flame-projection delay time versus the fuel flow rate for the establishment of external combustion in underventilated compartment fires. Bertin et al. [13] also studied the wall fire behavior in an underventilated room using a vertical porous flat burner located at the rear wall. Lattimer et al. [14] studied the flame spread and HRR of a fire located in a corner with a combustible lining. These studies indicate that when the fuel location changes, the HRR significantly changes for an overventilated fire and time to flashover changes. There have been few studies however, of the effects of fuel location and distribution on detailed fire dynamics and structure including the spatial distributions

of temperature and combustion products in an underventilated compartment fire.

Recently, Thomas et al. [4] investigated the effects of fuel quantity and location on ethanol pool fires in an ISO 9705 room. In this study, a fuel package consisting of two or three burners was placed inside the door (front), in the center of the room (center), or adjacent to the back wall (back). They found that the variation of fuel location resulted in significant changes in time histories of HRR and temperature as well as their maximum values. For maximum HRRs, the ranking of the maximum HRR with the change in fuel location was observed to be  $HRR_{\text{front}} > HRR_{\text{back}} > HRR_{\text{center}}$ . This was thought to be due to difference in the combined effects of radiation feedback from the compartment walls and enhanced mixing with oxygen due to changes in fuel location. Considering that they used a full doorway, 0.8 m wide  $\times$  2.0 m high, a maximum fuel amount of 40 L, and a total burner surface corresponding to 1.0 m<sup>2</sup>, it can be estimated that the experiments were conducted in the overventilated fire regime [6]. In the field of fire safety engineering, it has been observed that underventilated fires may yield as much as 10 times more toxicants, such as CO, compared to overventilated fires [15,16]. There has been little detailed information regarding the change in the thermal and chemical environment in underventilated compartment fires as fuel is placed at different locations within a room.

This article focuses on three underventilated compartment fires burning heptane in a recent experimental study conducted at the National Institute of Standards and Technology (NIST) to investigate the effects of fuel location and distribution on fire phenomena in full-scale compartment fires [6]. Global parameters such as HRR, combustion efficiency, and global equivalence ratio [17,18] were measured and local distributions of temperature, heat flux, and product concentrations including CO are considered in detail. The experimental measurements are supplemented with numerical simulations to enhance the understanding of fire dynamics induced by the change in fuel location and distribution for underventilated fire conditions. The fire dynamics simulator (FDS, version 5.1.6, SVN 1710) [19] utilizing Large Eddy Simulation was employed in this study.

## DESCRIPTION OF EXPERIMENTS

Figure 1 presents the full scale enclosure based on a standard ISO 9705 room, which is 2.4 m wide  $\times$  3.6 m deep  $\times$  2.4 m high. A doorway of 0.2 m wide  $\times$  2.0 m high (1/4 doorway width compared to a full ISO

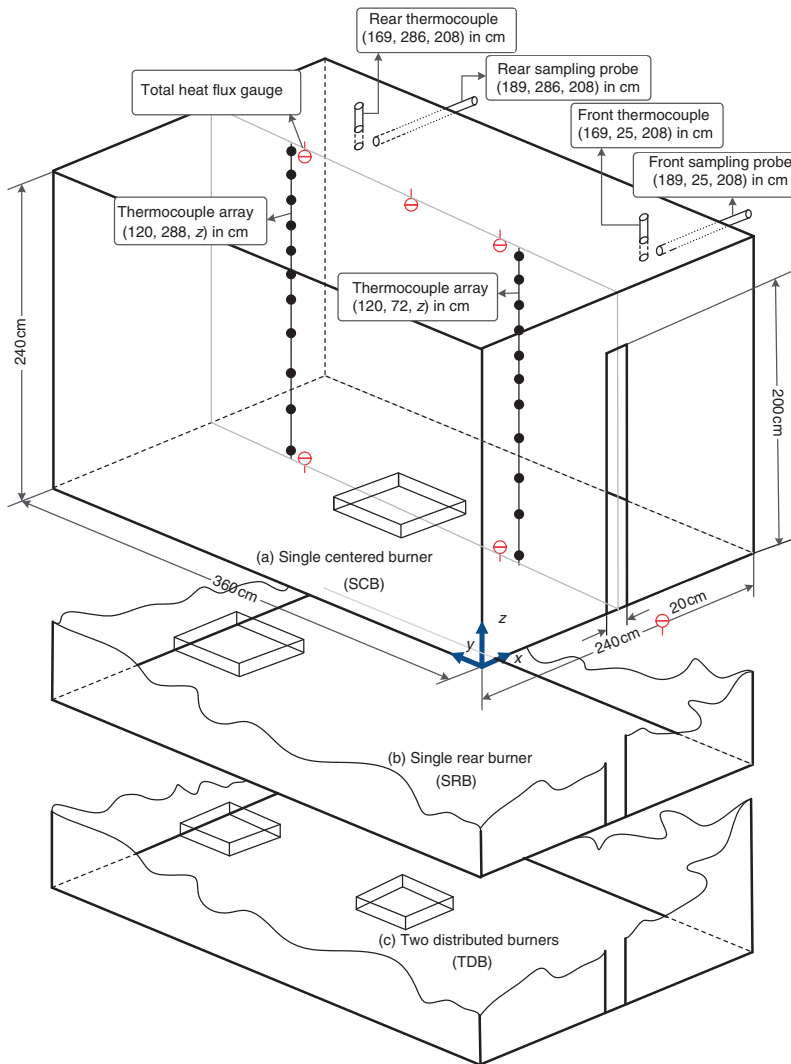


Figure 1. Schematic diagram of the ISO 9705 room for three fire tests of (a) single centered burner, (b) single rear burner, and (c) two distributed burners.

9705 doorway width of 0.8 m) centered at the bottom of the front wall was used to force the room to reach underventilated conditions with a smaller fire size. The uncertainty of the enclosure was measured as  $\pm 0.02$  m. The floor of the enclosure was raised 0.35 m above the ground to facilitate instrumentation. The support structure of the

enclosure was built using 0.89 mm (20 gauge) steel, structural studding, and 0.89 mm sheet steel. The floor of the structure was constructed of 4.8 mm thick steel sheet metal. The compartment walls, floor, and ceiling were covered with two layers of 25 mm (50 mm total) thick, 128 kg/m<sup>3</sup>, high temperature ceramic fiber blanket.

Temperature and species concentrations including O<sub>2</sub>, CO, CO<sub>2</sub>, and total hydrocarbons were continuously measured at the front and rear positions of the upper layer in the compartment. Type-R thermocouples with a bead diameter of 0.5 mm ± 0.125 mm were installed to measure the temperatures of the upper layer. Oxygen was measured using paramagnetic analyzers (Servomex<sup>1</sup>, 4100), carbon monoxide, and carbon dioxide were measured using nondispersive infrared analyzers (Siemens, Ultramat 6E). Total hydrocarbons were measured using two flame ionization detectors (Baseline-Mocon, 8800 H). A gas chromatograph was also used intermittently during some of the tests at the front and rear sampling locations to provide additional gas species information and to ensure reliability of gas species measurements. The measurements of all gas species are reported on a wet basis in this article. Two liquid cooled probes were used to sample gas inside the compartment at the front and rear locations. Detailed locations are indicated in Figure 1. The sampling probes, 3 m in length, were constructed of three concentric stainless steel (type 304) tubes. Water was forced through the inner shell and returned through the outer shell. The inner diameter of the sample probe was 4.0 mm. This design allowed the cooling fluid to condition the entire length of the probe. The relatively cool probe temperature assured that chemical reactions were frozen in the sampling lines. To measure the vertical thermal profiles within a compartment, two arrays of 11 type-K thermocouples with a bead diameter of 1.0 ± 0.25 mm were utilized. Thermocouples were placed at 0.03, 0.30, 0.60, 0.90, 1.05, 1.20, 1.35, 1.50, 1.80, 2.10, and 2.38 m above the floor. In addition, six total heat flux gauges, 6.4 mm diameter Schmidt-Boelter type, water cooled gauges were installed on the ceiling and floor as listed in Table 1. A full description of the experimental apparatus and additional instrumentation including total expanded uncertainty for each measurement is given in NIST Technical Note 1603 [6].

HRR measurements were conducted using the 6 m × 6 m calorimeter at the NIST Large Fire Research Laboratory (LFRL) [20]. The HRR

---

<sup>1</sup>Certain commercial entities, equipment, or materials may be identified in this document in order to describe an experimental procedure or concept adequately. Such identification is not intended to imply recommendation or endorsement by the National Institute of Standards and Technology, nor is it intended to imply that the entities, materials, or equipment are necessarily the best available for the purpose.

Table 1. Locations of total heat flux gauges.

	Location	x (m)	y (m)	z (m)
Ceiling	Front	1.20 ( $\pm 0.02$ m)	0.90 ( $\pm 0.02$ m)	2.33 ( $\pm 0.02$ m)
	Center	1.20 ( $\pm 0.02$ m)	1.78 ( $\pm 0.02$ m)	2.33 ( $\pm 0.02$ m)
	Rear	1.20 ( $\pm 0.02$ m)	2.66 ( $\pm 0.02$ m)	2.33 ( $\pm 0.02$ m)
Floor	Front	1.20 ( $\pm 0.02$ m)	0.90 ( $\pm 0.02$ m)	0.00 ( $\pm 0.02$ m)
	Rear	1.20 ( $\pm 0.02$ m)	2.66 ( $\pm 0.02$ m)	0.00 ( $\pm 0.02$ m)
	Outside	1.20 ( $\pm 0.02$ m)	-0.20 ( $\pm 0.02$ m)	0.00 ( $\pm 0.02$ m)

measurements were based on the oxygen consumption calorimetry principle with the assumption that a known amount of heat is released for each gram of oxygen consumed by a fire. The measurements of exhaust flow velocity and species volume fractions ( $O_2$ ,  $CO_2$ , and  $CO$ ) were conducted to determine the HRR based on the formulation derived by Parker [21]. The total expanded relative uncertainty of the HRR measurements reported was  $\pm 14\%$  based on a propagation of uncertainty analysis.

This study examined three heptane fires. Different fuel locations and distributions were examined: a single centered burner (SCB), a single rear burner (SRB) and two distributed burners (TDB) as shown in Figure 1. Pan burner(s) were used and total burner surface area was fixed at  $0.5 \text{ m}^2$ . The pan burners had no forced feeding mechanism; the fuel was placed in the pan and allowed to burn freely. In the cases of SCB and SRB, a single burner size of  $0.707 \text{ m} \times 0.707 \text{ m}$  ( $0.5 \text{ m}^2$ ) with a 10 cm lip was positioned in the geometric center of the floor (SCB) and along the centerline of the room next to the rear wall (SRB). Two  $0.25 \text{ m}^2$  burners were placed at the center and rear locations in the TDB case. The total volume of fuel was fixed at 30 L ( $\approx 20 \text{ kg}$ ) for all cases. The fuel mass loss rate was measured using a load cell mounted underneath the burner with a measurement accuracy of  $\pm 0.001 \text{ kg}$ . A summary of the experimental conditions is listed in Table 2.

## DESCRIPTION OF NUMERICAL SIMULATIONS

To provide insight into the fire characteristics including details of the flow field for the underventilated compartment fires, numerical simulations were performed using FDS (ver. 5.1.6, SVN 1710). This article should not be considered a validation study. A detailed description of FDS and its validation is given in [19]. FDS numerically solves a form of the Navier-Stokes equations for low-speed, thermally-driven flow with an emphasis on smoke and heat transport from fires.

Table 2. Summary of experimental conditions and global parameters.

	Single centered burner (SCB)	Single rear burner (SRB)	Two distributed burners (TDB)
Burner size (m <sup>2</sup> )	0.50 (±0.015)	0.50 (±0.015)	2×0.25 (±0.008)
Fuel mass (kg)	20 (±0.1)	20 (±0.1)	2×10 (±0.1)
Duration (s)	600	600	600
Pseudo-steady state period (s)	200~500	200~500	200~500
Ideal heat release rate (kW)	1830 (±110)	1750 (±105)	1660 (±100)
Measured heat release Rate (kW)	1480 (±207)	1420 (±200)	1330 (±187)
Combustion efficiency (%)	81 (±12.3)	81 (±12.4)	80 (±12.3)
Fuel mass loss rate (kg/s)	0.041 (±0.001)	0.039 (±0.001)	0.037 (±0.001)
Air mass flow rate into door (kg/s)*	0.288	0.288	0.297
Global equivalence ratio	2.16 (±0.008)	2.06 (±0.007)	1.89 (±0.006)
Global CO emission (ppm)**	134 (±16.0)	120 (±14.4)	130 (±15.9)

\*Air mass flow rates into doorway were calculated using the numerical results.

\*\*Global CO emission was measured at exhaust stack.

These equations are discretized in space using second order central difference and in time using an explicit, second order, predictor-corrector scheme. Radiative heat transfer is considered by solving the finite-volume-based radiation transport equations [22]. Large eddy simulation is utilized and the original Smagorinsky eddy viscosity model is used as the sub-grid scale turbulence model. Other than specifying physical properties and dimensions, fuel properties, mass loss rates, and soot loading all default FDS options were used. A customized post processing algorithm was utilized on the FDS output files to produce the averaged steady state results presented here.

The sub-grid scale combustion model in the previous FDS version used only a single mixture fraction variable which is defined as the mass fraction of the gas mixture that originates in the fuel stream. FDS (version 5), decomposes mixture fraction into three components to account for local flame extinction and the production/destruction of CO. Floyd et al. [23,24] reported on model validation for reduced scale enclosure experiments. They illustrated the accuracy of the CO model, in which some discrepancies between experiments and model still exist. In particular, when the fire became more underventilated, under-prediction of CO was observed. Detailed analysis using FDS is of value and is used here to help understand compartment fire phenomena.

The computational domain was extended beyond the outside of the compartment in order to take into account air entrainment through the doorway and burning outside the compartment in underventilated conditions. The computational domain was set with dimensions of

2.40 m (x)  $\times$  6.96 m (y)  $\times$  4.47 m (z) as shown in Figure 2. Nonuniform grid and multi-domains were used to reduce the total grid numbers. Approximately 600,000 total grid cells were used and the average grid size ( $\bar{\Delta}$ ) was approximately 0.05 m. Note that an additional grid set of  $\bar{\Delta} = 0.015$  m was inserted near the doorway to resolve the large gradients there. Detailed numerical validation for these underventilated compartment fires (corresponding to the SCB case in the current study) including the grid sensitivity results can be found in a previous study [25]. The measured fuel mass loss rates were used as the model input of the fire source. The soot yield, which represents the fraction of fuel mass converted into smoke particulate, was prescribed using a value of 0.015 to approximate the soot generation in heptane fires [26]. The heat transfer boundary condition on the walls was prescribed using the temperature-dependent properties of the ceramic fiber blanket [27]. Open boundary conditions were imposed at the external boundaries and the wall boundary conditions were used at the walls, ceiling and floor.

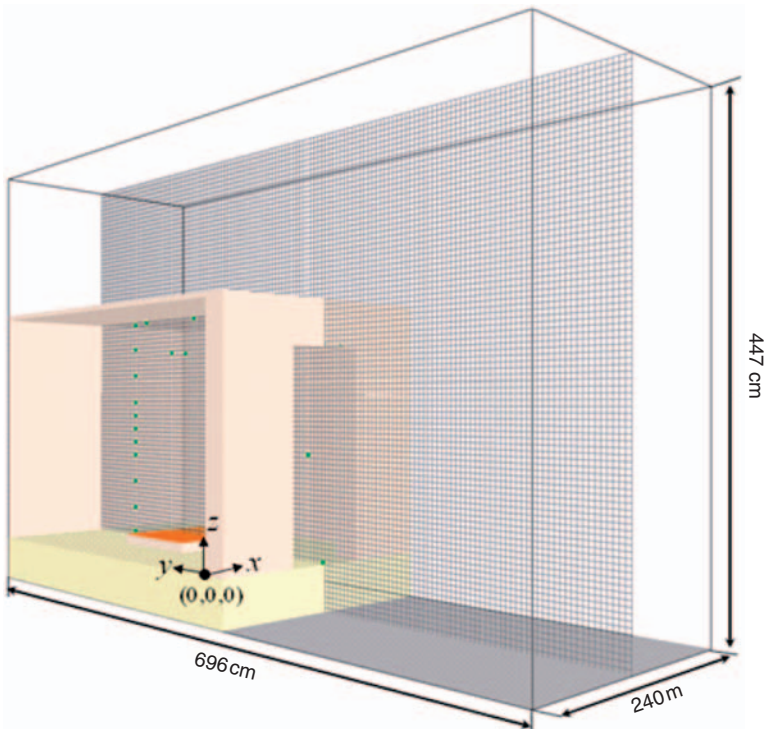


*Figure 2.* Computational domain for FDS simulation of fire dynamics in the ISO 9705 room.

## RESULTS AND DISCUSSION

### Experimental Results: Global Fire Characteristics

Figure 3 shows images of the compartment fire after ignition for three cases with different fuel locations and distributions. Images are presented at 50 s and 150 s after ignition. At 150 s, it is obvious that most of the burning occurred outside of the enclosure. Comparing the images of the fire at 50 s and 150 s, the SRB case has burning outside the

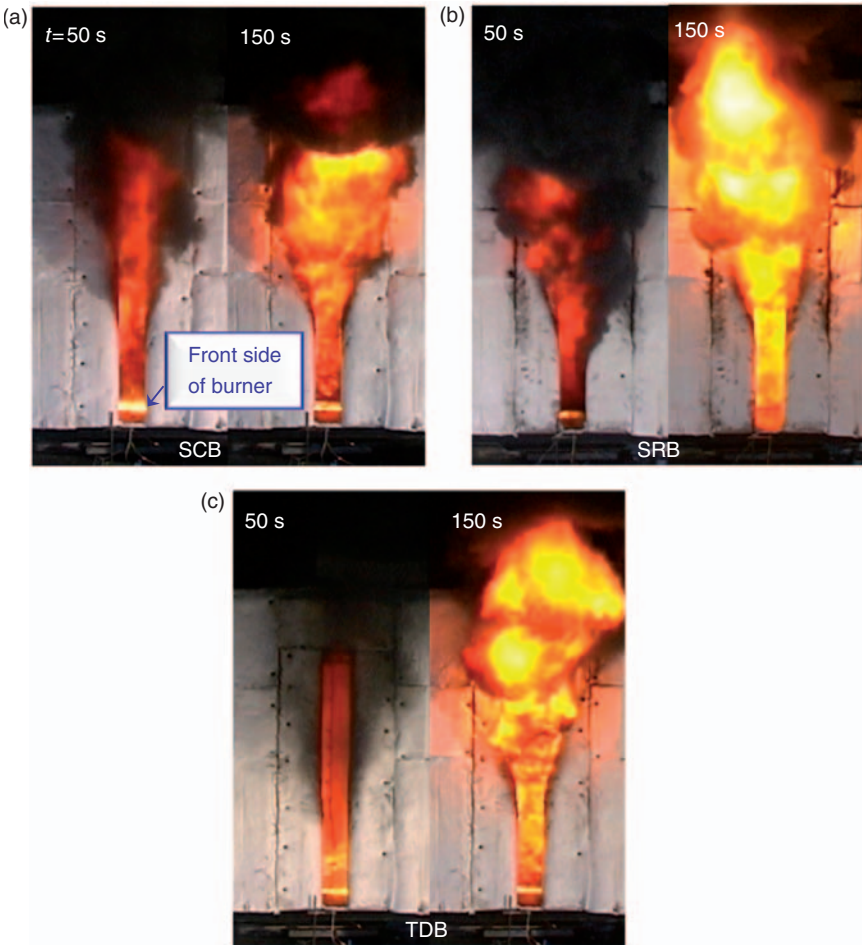


*Figure 3. Temporal images of compartment fire at 50 s and 150 s after ignition for three cases with different fuel locations and distributions (doorway width is 0.2 m).*

door earlier in the fire development than the other cases. This can be explained, in part, by the SRB case having the fuel located the furthest from the vent. When the burner was placed adjacent to the rear wall of the enclosure, the area through which air may be entrained was reduced and the overall fuel-air mixing rate decreased [28]. The restriction of air entrainment to the fire plume led to an increase in flame length, due to excess volatilized fuel. Consequently, the fire became underventilated earlier than the centered burner case (i.e., the SCB case). For the TDB case, smaller burners were placed at the center and rear of the compartment. The absence of external burning early was attributed to the locally decreased oxygen demand due to the distributed fuel as compared to the other cases allowing for more air to be entrained with the fuel. Even though the time to burning outside the room was different with the change in fuel placement, it was difficult to find distinct differences in flame shape once the fire was established in steady state, for example at  $t > 150$  s. In addition, it is interesting to note that a higher radiant intensity was observed near the front side of the burner in the cases of SCB and TDB. This phenomenon can be explained by the previous numerical study [25] that, in the case of SCB, the flame was only attached on the front side of the burner due to insufficient oxygen near the burner in the underventilated condition. High intensity radiation was not observed near the burner in the SRB case at 150 s. There are two possible explanations. First, the flame surface corresponding to a location of stoichiometric mixture fraction may not have occurred at the burner, but at other places inside the compartment because the burner was placed far from the vent. Thus, there was no high intensity radiation near the burner because there was little or no burning in the rear of the room. The second possibility is that, if the flame surface was attached on the front side of the rear burner, it may be difficult to distinguish the radiation originating from the burner to the radiation coming from the flame established near the doorway. This will be discussed in more detail in the 'Numerical Results' section.

Underventilated burning is controlled by oxygen transport. Changing the fuel distribution in the compartment may have led to changes in fuel volatilization rate and the chemical and thermal environment within a compartment. Figure 4 presents a comparison of fuel mass measured using a load cell mounted underneath the burner for the three cases with different fuel locations and distributions. For the TDB case, the fuel mass at the centered and rear burners was individually measured and the total value was plotted as the Total\_TDB. Prior to the fire becoming underventilated (before 50 s), the fuel mass loss rates for all cases were about 0.02 kg/s. After the fire becomes underventilated, the

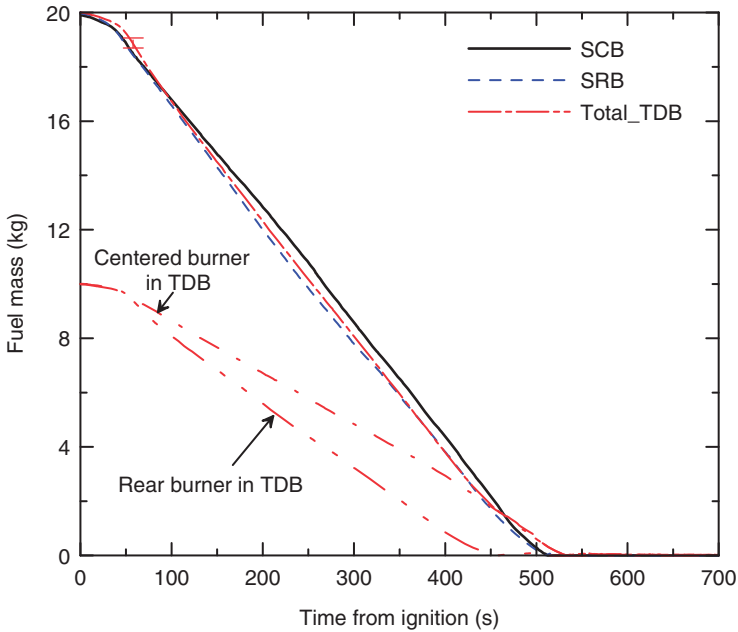


**Figure 4.** Comparison of fuel mass as a function of time for three cases with different fuel locations and distributions (each of the transient fuel masses at the centered and rear burner in the TDB case is also plotted).

fuel mass loss rates were about 0.04 kg/s. That is, the fuel mass loss rates in the underventilated fire were approximately twice that observed in the overventilated fire. This is attributed to the higher HRR in the underventilated condition. This result does not mean that larger amounts of fuel were consumed within the underventilated compartment compared to the overventilated compartment. In fact, most volatilized fuels cannot oxidize inside the compartment due to restricted air entrainment. In the TDB case, the fuel in the rear burner was volatilized more rapidly than in the center burner and the rear burner was experimentally observed to become empty before to the center burner (based on mass loss measurements, and visible observation). This can be explained by the combined effects of the radiative feedback from the adjacent enclosure walls and enhanced convective heat transfer on the burner surface. When the burner is placed near an enclosure wall, it has been shown that radiative feedback to burner surface can increase [4]. In addition, the different flow direction above the burner surface may lead to significant changes in convective heat transfer

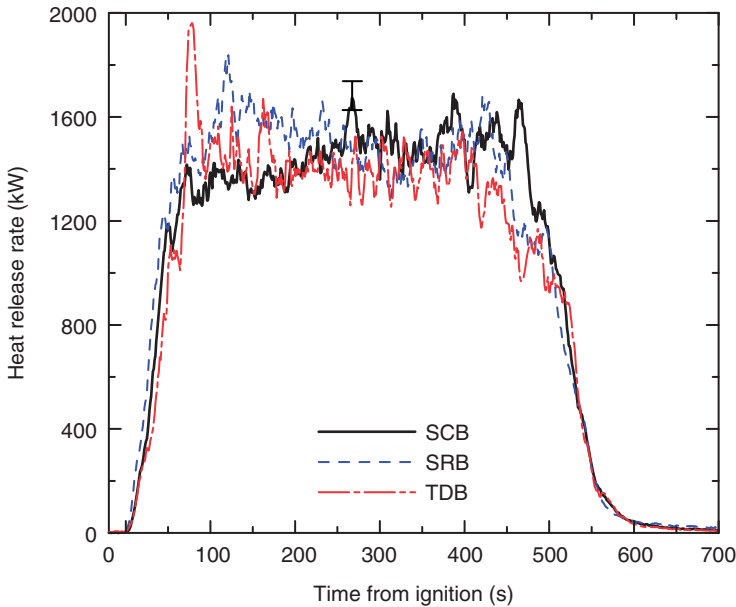


Figure 5. Comparison of heat release rates for three cases with different fuel locations and distributions.

(which will be illustrated in Figure 10). Therefore, the SRB case shows the fastest fuel volatilization while the SCB shows the slowest volatilization in the underventilated fire for the cases considered here. However, the differences in the global fuel mass loss rate for each case are not large.

Figure 5 shows a comparison of the HRRs for three cases with different fuel locations and distributions. In the pseudo-steady period, the average HRRs were nearly the same regardless of fuel location and distribution, which was to be expected since an identical quantity of fuel with identical burner area was used in all cases. However, the transient behavior of HRR shows some differences among the three cases. After ignition, each HRR rapidly increased for approximately 50 s, then oscillated slightly before becoming steady. This variation of HRR for a short period is related to the onset of underventilated conditions evidenced by flame extension outside the compartment. The SRB case showed the fastest onset of external burning while the TDB case showed the slowest onset of external burning, as seen in Figure 3. During the underventilated period, the HRR in the SCB case was initially smaller than the other cases and gradually increased to a maximum value near the end of the experiment.

On the other hand, the cases of SRB and TDB initially peaked in HRR and then proceeded to gradually decrease before dropping off rapidly after the fire burned out. From this figure, it can be seen that the change in fuel location and distribution brought about the change in transient behavior, including the onset of underventilated burning.

To confirm the variations in global fire characteristics as fuel was placed at different locations within a compartment, the HRR, combustion efficiency<sup>2</sup>, global equivalence ratio, and global CO emission outside the compartment are summarized in Table 2. The values in parentheses indicate the total expanded uncertainty for each measurement. The combustion efficiency was defined as the ratio of the measured HRR to the ideal HRR. The ideal HRR was calculated using measured fuel mass loss rate and the heat of combustion for heptane fuel (44.6 MJ/kg) [29]. The global equivalence ratio [30] was evaluated as  $\phi_g = (r_s/Y_{O_2,a}) \times (\dot{m}_f/\dot{m}_a)$ , where  $r_s$  is the stoichiometric oxygen-to-heptane mass ratio,  $r_s \approx 3.52$ ;  $Y_{O_2,a}$  the oxygen mass fraction in ambient air,  $Y_{O_2,a} \approx 0.233$ ;  $\dot{m}_f$  fuel mass loss rate;  $\dot{m}_a$  the air mass flow rate into the doorway from the ambient. Unfortunately, measurements of entrained air mass flow rate were not conducted for these experiments. Instead, the air mass flow rate into the doorway was calculated using predicted temperature and velocity from numerical simulations. The predicted average  $\dot{m}_a$  is nearly the same regardless of fuel location and distribution, 0.288 kg/s, 0.288 kg/s and 0.297 kg/s for SCB, SRB, and TDB, respectively. For reference, the inflow of air estimated by  $\dot{m}_a \approx 0.52A_o\sqrt{h_o}$ , where  $A_o$  and  $h_o$  are the area and height of the doorway opening [28], is  $\dot{m}_a = 0.294$  kg/s for the compartment configuration used in the current study. This value is very close to the numerically calculated value and shows that the air mass flow rate is reasonable. These results imply that the overall steady state burning characteristics are similar inside the compartment for each fire since the fuel mass loss rate is nearly the same, as illustrated in Figure 4. Although the averaged ideal and measured HRRs show some differences during the pseudo-steady period for each case, the combustion efficiency is nearly the same at 80% regardless of the fuel placement. The global equivalence ratio has a similar value for each case, 2.16, 2.06, and 1.89 for the SCB, SRB, and TDB, respectively. In addition, the global CO emission measured at the exhaust hood also has a similar value for each

<sup>2</sup>The combustion efficiency, as discussed here, is based on the measured fuel loss rate and the globally measured HRR rate of burning both inside and outside of the compartment. We are not able to separate the contribution of internal and external burning to the HRR measurement with our current equipment.

case, within 10%. Based on these observations, variations in fuel location and distribution do not play an important role in the global characteristics of underventilated compartment fires, for example, fuel mass loss rate, HRR, combustion efficiency, global equivalence ratio, and global CO emission outside the compartment. Therefore, the distributed fuel underventilated fire behavior is different than the distributed fuel overventilated fire behavior which is accompanied by the significant changes in global fire characteristics with fuel location varied [4].

### **Experimental Results: Local Characteristics of Thermal and Chemical Environments**

Although the overall characteristics of underventilated fires were not significantly affected by changes in fuel location and distribution, the local thermal and chemical environments may change inside the compartment. Thus, the local distributions of temperature, total heat flux, and gas species are discussed in this section.

Figure 6 shows a comparison of averaged steady state temperatures measured at the front and rear thermocouple array locations as a function of the height above the floor. The front and rear thermocouple arrays were at  $y = 0.72$  m and  $y = 2.88$  m on the centerline of  $x = 1.20$  m. In this figure, the vertical profile of temperature at the front location is the same within the uncertainty of the measurement, regardless of fuel location and distribution except for the minor difference at  $z = 0.025$  m, which indicates that the thermal environments of the three cases were nearly identical. The low temperatures,  $250^{\circ}\text{C}$  to  $400^{\circ}\text{C}$ , are located near the floor since there is air entrainment in this region. At the rear location, high temperatures ( $>800^{\circ}\text{C}$ ) are measured at all locations. The high temperatures near the floor indicate that products of high temperature exist in this region. The SRB and TDB cases show a similar rear vertical temperature profile, while the SCB case differed significantly. Consequently, the fuel placement had a greater influence on the temperature profile in the rear of the enclosure than in the front of the enclosure.

The temperature variations between SCB, SRB, and TDB were also observed in the average temperatures measured at the front and rear sampling probe locations (Table 3). A process of time average was conducted during the pseudo-steady period. The values in parentheses indicate the total expanded uncertainty for each measurement. At the front sampling location, a maximum difference in temperature of  $60^{\circ}\text{C}$  between the SRB and the TDB case is observed, while the cases of SCB and SRB show the maximum difference of  $110^{\circ}\text{C}$  at the rear sampling location. The cause is

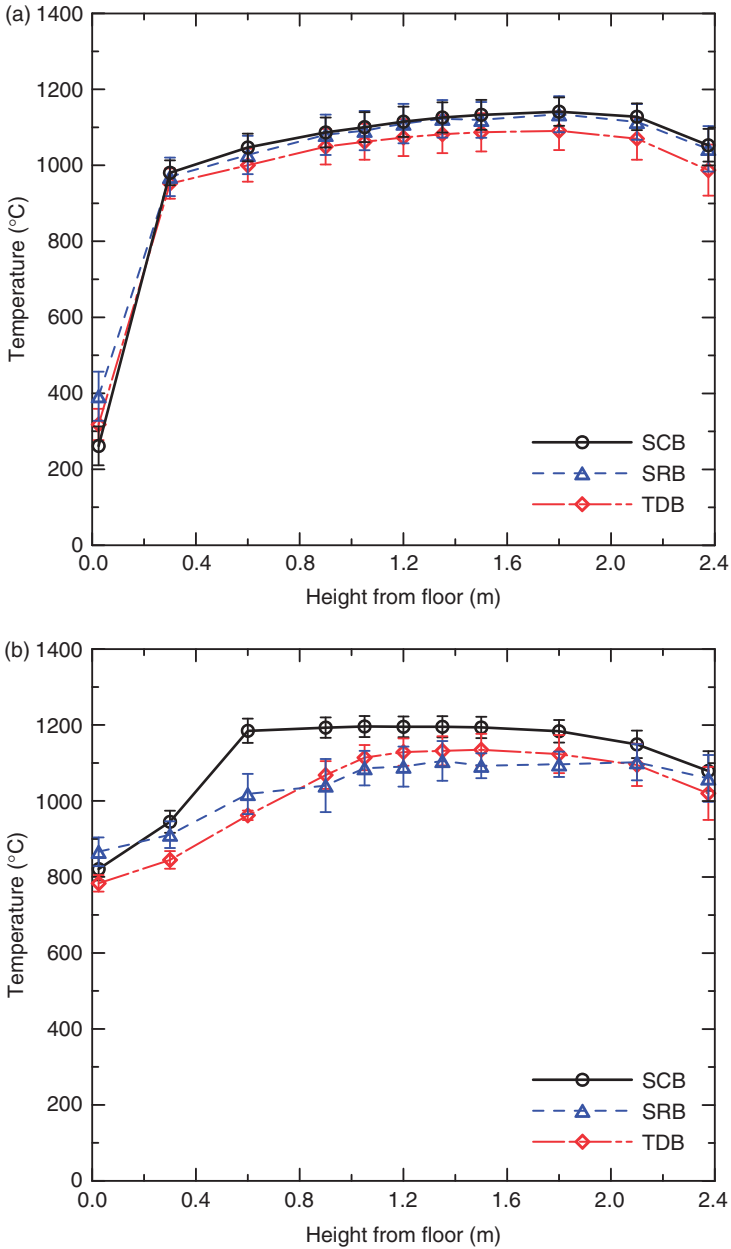


Figure 6. Comparison of averaged temperatures measured at front and rear thermocouple arrays as a function of the height from the floor: (a) at front TC array, (b) at rear TC array.

Table 3. Experimental data of averaged temperatures and species volume fractions.

At the front sampling probe location			
	SCB	SRB	TDB
T (°C)	1070 (±64)	1090 (±65)	1030 (±62)
$x_{O_2} (\times 10^3)$	0.284 (±0.0340)	0.220 (±0.0264)	0.758 (±0.0910)
$x_{CO_2}$	0.078 (±0.0094)	0.074 (±0.0088)	0.087 (±0.0104)
$x_{CO}$	0.041 (±0.0049)	0.045 (±0.0054)	0.034 (±0.0041)
At the rear sampling probe location			
	SCB	SRB	TDB
T (°C)	1130 (±68)	1240 (±74)	1140 (±68)
$x_{O_2} (\times 10^3)$	0.448 (±0.0537)	4.232 (±0.5078)	4.845 (±0.5815)
$x_{CO_2}$	0.069 (±0.0082)	0.094 (±0.0113)	0.093 (±0.0111)
$x_{CO}$	0.050 (±0.0060)	0.022 (±0.0026)	0.024 (±0.0029)

not clear since the temperature distribution is complexly related to the three-dimensional flame and flow structures inside the compartment.

Figure 7 presents a comparison of total heat fluxes as a function of time at the front and rear floors. This comparison of total heat flux measurements for each case shows the variations in thermal environment with time inside the compartment. After ignition, each total heat flux rapidly increases to an initial peak at approximately 50 s, then the signal drops slightly and continues to slowly increase throughout the experiment. The reduction in heat flux after the initial peak indicates the onset of underventilated burning and exhibits qualitative similarities to the HRR transient behavior shown in Figure 5. Near the end of the experiment ( $\approx 500$  s), the total heat fluxes sharply increase up to the maximum values for all cases because of the decrease in global equivalence ratio due to decreased fuel concentration and increased oxygen concentration inside the compartment, resulting in brief well-ventilated fire behavior. At the front location (between the doorway and the centered burner), the total heat flux gradually increased in the pseudo-steady period and all cases showed similar transient behavior. At the rear location (between the centered burner and the rear burner or the rear wall), the change in fuel placement led to significant variation in the transient total heat flux. The SRB case shows a gradual increase in the total heat flux as time increased, while the SCB and TDB cases, which had the centered burner, have nearly constant total heat flux values in the pseudo-steady period. The different transient behaviors of each case may be explained by a flame location and existence/nonexistence of the center burner. Considering that the fuel mass loss

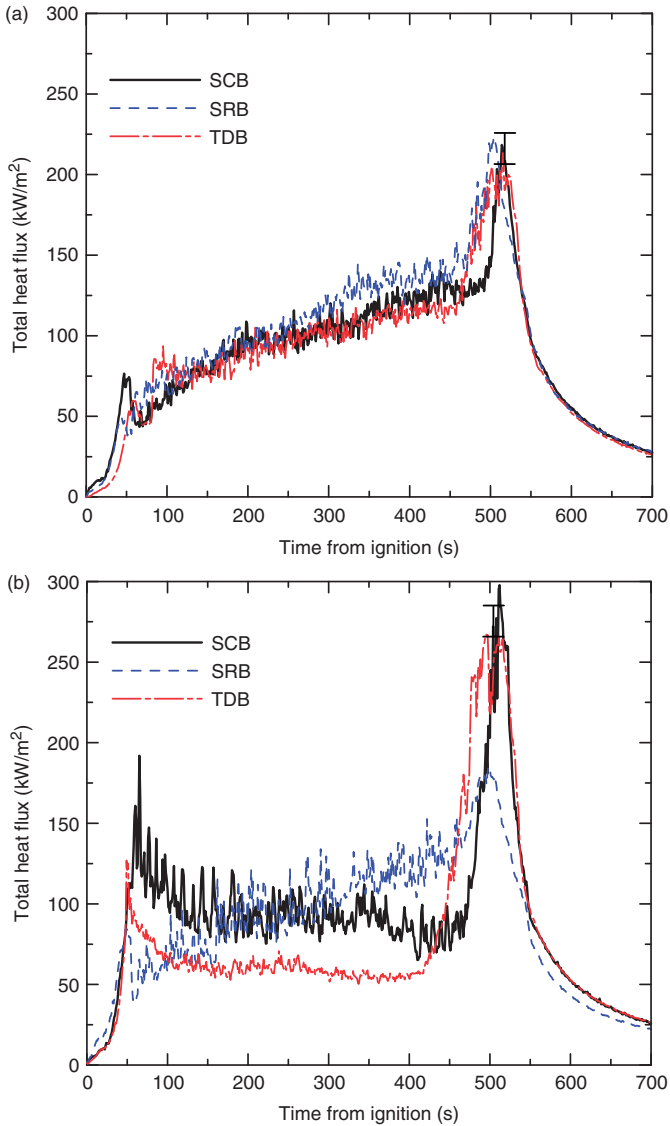


Figure 7. Comparison of total heat fluxes as a function of time at the front and rear floor: (a) at front floor, (b) at rear floor.

rate and the entrained air mass flow rate were similar for all cases, as identified in Figure 3 and Table 2, the flame location near the floor was nearly identical regardless of fuel location and distribution. Numerical results (discussed in later) also indicate that the flame is attached on the

front side of the center burner in the case of SCB and TDB, and also positioned at nearly the same location ( $y \approx 1.6$  m) in the SRB case. So, the total heat flux gauges in all cases were nominally located at the same distance from the flame surface. In the cases of SCB and TDB, a radiative heat originating from the flame surface was absorbed by the liquid fuel resulting in heating and vaporization. Consequently, the total heat flux at the rear location was nearly the same value throughout the experiment. However in the case of SRB, the total heat flux gradually increased, similar to the transient behavior observed at the front location. Based on the thermocouple array data presented in Figure 6, it can be concluded that the thermal environment in the front of the enclosure was quite similar for each case. This led to similar heat flux values measured for each case. On the other hand, the change in location and distribution of the burner(s) brought about a significant change in thermal environment in the rear of the enclosure.

To examine the effect of fuel location and distribution on the chemical environment inside the compartment, Figure 8 presents a comparison of CO<sub>2</sub> volume fraction at the front and rear sampling probe locations. Although the O<sub>2</sub> concentration is not presented in this article, the O<sub>2</sub> volume fraction was nearly zero in the pseudo-steady period due to the underventilated conditions in all cases. The CO<sub>2</sub> volume fraction at the front sample location (Figure 8(a)) increased initially and then gradually decreased with time for each case. Even though the difference in CO<sub>2</sub> volume fraction in each case increased with time, the difference among three cases is not large. A larger difference in CO<sub>2</sub> volume fraction was observed at the rear sampling probe location (Figure 8(b)). While the SRB and TDB cases showed nearly constant CO<sub>2</sub> volume fractions in the pseudo-steady period, the CO<sub>2</sub> volume fraction in the SCB case decreased significantly with time compared to the other cases. This result indicates that the amount of incomplete combustion gradually increased with time, especially in the rear of the enclosure for the SCB case.

Figure 9 compares the measured CO volume fraction at the front and rear sampling locations within the enclosure. At the front sampling location (Figure 9(a)), CO concentration gradually increased with time for each case. The transient CO behavior for each case shows the opposite trend to the CO<sub>2</sub> behavior, as expected. At the front sampling location, the difference in CO volume fraction among the cases was not large and was similar to that of CO<sub>2</sub>. On the other hand, at the rear sampling location (Figure 9(b)), CO increased significantly in the SCB case with time, while the SRB and TDB cases showed steady CO concentration throughout the period of steady burning. Figures 8 and 9 indicate that the variation in fuel placement played a more important

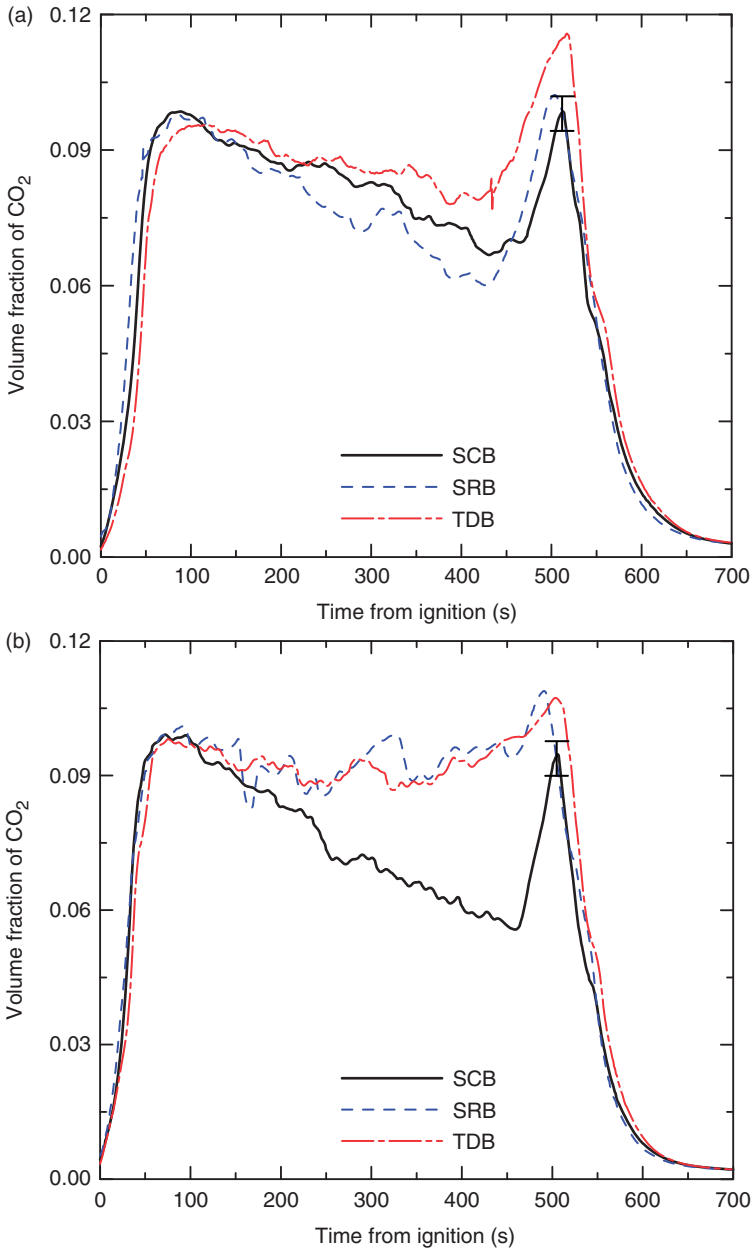
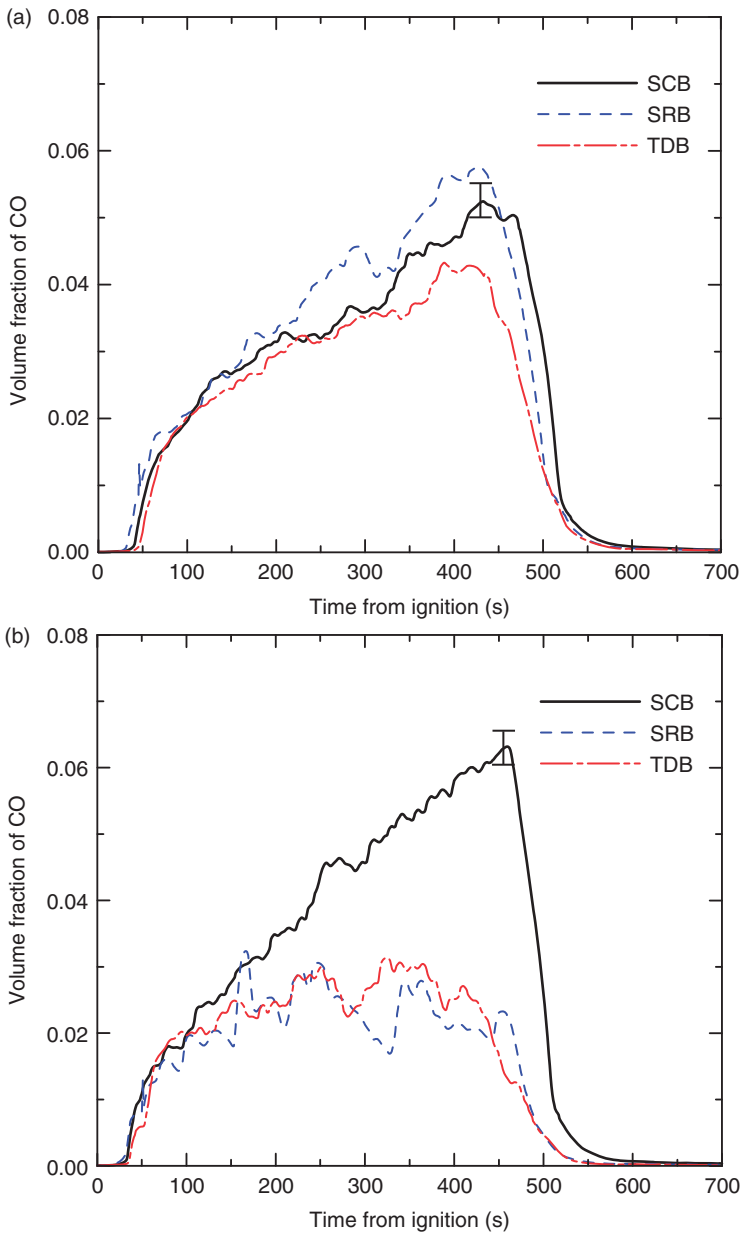


Figure 8. Comparison of CO<sub>2</sub> volume fractions at the front and rear sampling probe locations: (a) at front sampling location, (b) at rear sampling location.



**Figure 9.** Comparison of CO volume fractions at the front and rear sampling probe locations: (a) at front sampling location, (b) at rear sampling location.

role in the change in chemical environment in the rear of the compartment than in the front. This was also observed in the average species volume fraction (Table 3). The  $O_2$  volume fraction was very small in both the front and rear locations. The maximum differences in  $CO_2$  and CO volume fractions between the front and rear sampling locations were 0.013 and 0.026, respectively. That is, the change in fuel location and distribution was accompanied by larger changes in CO and  $CO_2$  volume fraction at the rear sampling location than at the front location. It is difficult to explain the cause of these differences with the data measured at only two local sampling locations. In a previous study [25], it was observed that product sampling at local positions in the upper layer cannot represent the fire characteristics in underventilated conditions. In particular, the CO in the underventilated compartment fire was directly related to the three-dimensional flow structure and the  $O_2$  distribution. Therefore, the details of CO with the change in fuel placement will be discussed in the context of three-dimensional fire behaviors based on numerical simulations.

### **Numerical Results: Multi-dimensional Fire Behavior**

Numerical validation of the SCB case was conducted previously [25] and compared with experimentally measured temperature, heat flux,  $O_2$ ,  $CO_2$ , CO, and total hydrocarbon volume fractions. The current numerical approach provides a semi-qualitative comparison to experimental results observed in the underventilated compartment fire. In this section, the examination of multi-dimensional fire behavior focuses on understanding the variation in the thermal and chemical environments including flow dynamics as the fuel location and distribution changed within the compartment.

Figure 10 presents the HRRPUV (Heat Release Rate Per Unit Volume) color contours, velocity vectors, and flow streamlines on the  $y$ - $z$  plane at  $x = 1.2$  m for each of the three cases. The plots represent time-averaged results over a period of 300 s during pseudo-steady state burning, as listed in Table 2. The HRRPUV contours ranged from 100 to 2,000 kW/m<sup>3</sup>. A mean flame surface line at a stoichiometric mixture fraction value ( $Z_{st}$ ) of 0.0622 for a heptane fire [31,32] is also plotted. To help understand the flow field, the  $y$ -velocity ( $V$ ) of zero is also shown with a blue line. In the SCB case, the flame is only attached on the front side of the centered burner and most burning occurs outside the compartment. The internal flow can be classified into two patterns. On the basis of the zero velocity line, the flow exhausted toward the doorway in the front region, while the flow circulated along the ceiling, down the back wall and across the floor.

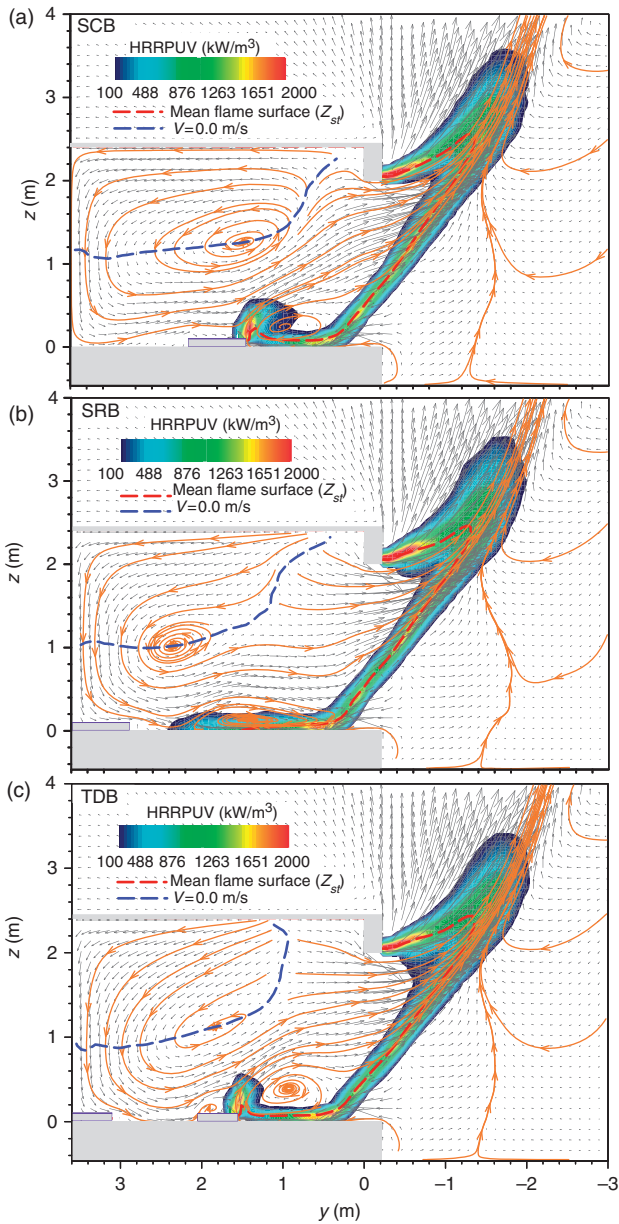


Figure 10. Mean calculated distributions of HRRPUV, velocity vector and flow streamlines on the  $y$ - $z$  plane at  $x = 1.2$  m.

This indicates that a portion of products formed near the doorway circulated counterclockwise inside the compartment. This flow pattern may have accelerated a fast fuel volatilization by enhanced convective heat transfer. For the SRB and TDB cases, the distribution of HRRPUV is very similar to that in the SCB case and the location that the flame surface meets the floor is nearly the same ( $y \approx 1.6$  m) regardless of the fuel distribution. This supports the idea that there are minimal differences in the different cases during steady underventilated burning. The flame location as well as the HRRPUV distribution in the front of the compartment is consistent with the experimental results that the variation in the fuel placement does not play an important role in the thermal and chemical environment in the front of the compartment. Despite the lack of a strong relationship between fuel placement and the conditions in the front region of the compartment, the center of rotation inside the compartment is positioned at different locations depending on the fuel placement. The change in the location of the center of rotation indicates differences in the rear flow field. Changes in the rear flow field may result in changes in the thermal and chemical environment as well, as shown in Figures 6–9. The existence of a rear burner in the SRB and TDB cases may also cause a significant change in the distribution of volatilized fuel compared to the SCB case.

Figure 11 shows the mean distributions of temperature on the  $y$ - $z$  plane at  $x = 1.2$  m. In all cases, the highest temperature was near the front floor of the compartment because of the oxygen supply from the doorway supporting a flame there. The temperature inside the compartment gradually decreased along the path of the rotating flow. Two possible hypotheses for this effect were discussed previously including lower flame temperatures in fuel-rich fires and an endothermic reaction of  $\text{CO}_2$ -dissociation [25]. The distributions of predicted temperature are very similar regardless of the fuel placement inside the compartment except for minor differences near the burner due to fuel volatilization. This helps explain the experimentally observed differences at the rear location discussed above (Figure 6). Partially premixed burning and thermal decomposition of volatilized fuel may be occurring as well. However the current chemical submodel in FDS is unable to capture that detail.

Figure 12 illustrates the three-dimensional distributions of mean mixture fraction and flow streamlines. The distribution of mixture fraction was expressed with three iso-contours, that is, 0.250 ( $Z_1$ ), 0.120 ( $Z_2$ ), 0.0622 ( $Z_{st}$ ). The flow streamlines started at three points ( $x = 1.15$  m, 1.20 m and 1.25 m) near the bottom of the doorway for all cases. The three-dimensional behavior of the flow is obvious from these streamlines. The blue dots on the streamline have a constant spacing in

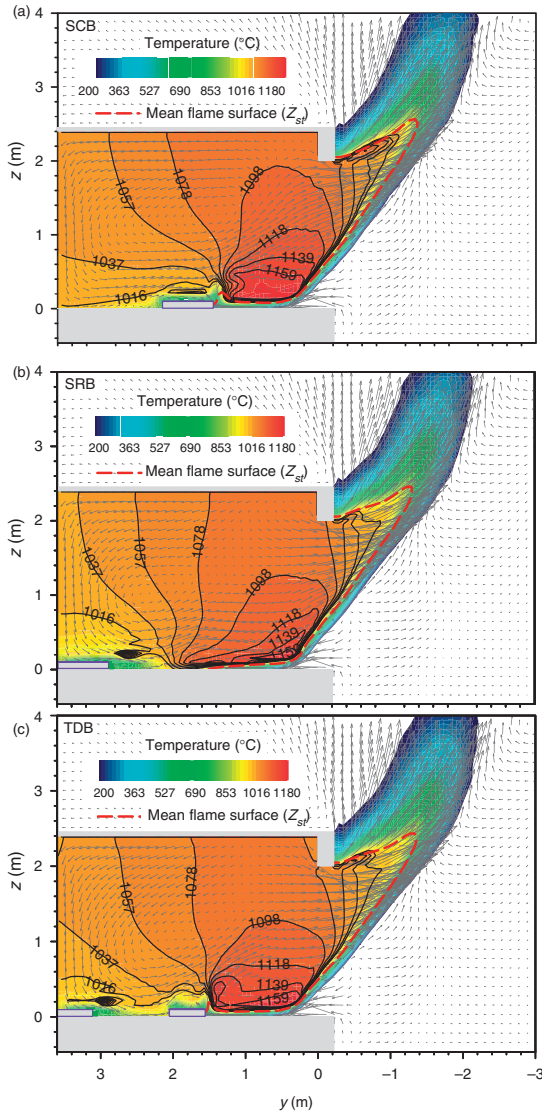


Figure 11. Mean calculated distributions of temperature on the  $y-z$  plane at  $x = 1.2$  m.

time at an interval of 0.5 s. That is, a greater streamline length between two dots indicates that a fluid velocity is higher than that in other regions having a smaller streamline length between two dots. In this figure, the mean flame surface ( $Z_{st} = 0.0622$ ) is distributed at nearly the

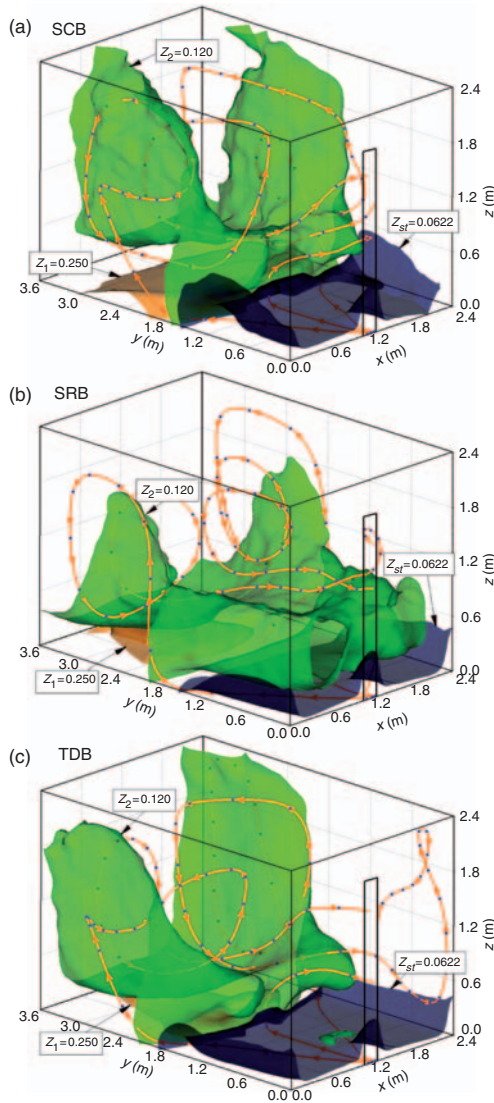


Figure 12. Three-dimensional distributions of mean mixture fraction and flow streamlines inside the compartment.

same location regardless of fuel distribution, similar to what is shown in Figure 10. For the iso-contour of  $Z_1 = 0.250$  corresponding to a high fuel concentration, the distribution of the iso-mixture fraction significantly changed based on the location of the fuel inside the compartment.

In the SCB case, the  $Z_1$  surface was distributed in the range of  $1.8\text{ m} < y < 3.0\text{ m}$ , and in the ranges of  $2.1\text{ m} < y < 3.6\text{ m}$  and  $1.8\text{ m} < y < 3.6\text{ m}$  for the SRB and TDB cases, respectively. For the iso-contour of  $Z_2 = 0.120$ , the fuel concentration near the side wall of the compartment is higher than that near the center region. The SCB and TDB cases show a similar mixture fraction distribution, while the SRB case yields a different distribution. Specifically, in the SRB case, a higher fuel concentration was located in the front region compared to the SCB and TDB cases. This phenomenon can be explained by the relative shift of the rotating core toward the rear of the compartment in the SRB case, as shown in Figure 10. That is, in the SRB case, more volatilized fuel was transported to the front because of the higher magnitude of velocity in the rear of the compartment when compared to the SCB and TDB cases. This result can be also confirmed by the three-dimensional flow streamlines. The SCB and TDB cases have an identical flow structure, while the case of SRB shows a different flow pattern inside the compartment. As a result, it can be concluded that cases with a center burner have different flow patterns than cases without a center burner, with consequent differences in thermal and chemical environments including the distribution of volatilized fuel within the room.

Figure 13 presents the predicted three-dimensional distributions of CO volume fraction inside the compartment for each case. Five CO volume fraction iso-contour levels are plotted between  $X_{CO} = 0.035$  and  $X_{CO} = 0.055$ . For the SCB case, the CO volume fraction is greatest in three regions inside the compartment; a region between the front side of the burner and the doorway, near the front ( $y \approx 1.2\text{ m}$ ) of the side walls and near the rear ( $y \approx 2.4\text{ m}$ ) of the side walls. The CO near the side walls can be attributed to the flame surface and flow streamlines in Figure 12. When the products generated near the front of the side wall rose toward the ceiling, the CO volume fraction at  $y \approx 1.2\text{ m}$  gradually increased due to an increasingly rich fuel-air mixture. Next, when the rising products circulated in the range of  $1.8\text{ m} \leq y \leq 3.0\text{ m}$ , the maximum CO volume fraction was located in the center region ( $y \approx 2.4\text{ m}$ ) of the circulation due to the penetration of the excess remaining  $O_2$  and long residence time under the high temperature conditions. This is a possible explanation of why the CO volume fraction was higher and the  $CO_2$  volume fraction is lower at the rear sampling probe location than at the front location, as presented in Figures 8 and 9 and Table 3. The TDB case shows a qualitatively similar CO distribution to the SCB case. In particular, the location of CO volume fraction at the rear circulating region ( $y \approx 2.4\text{ m}$ ) and the three-dimensional flow field, (Figure 12), were very similar between the SCB and TDB cases. The quantitative difference in CO concentration can be attributed to the

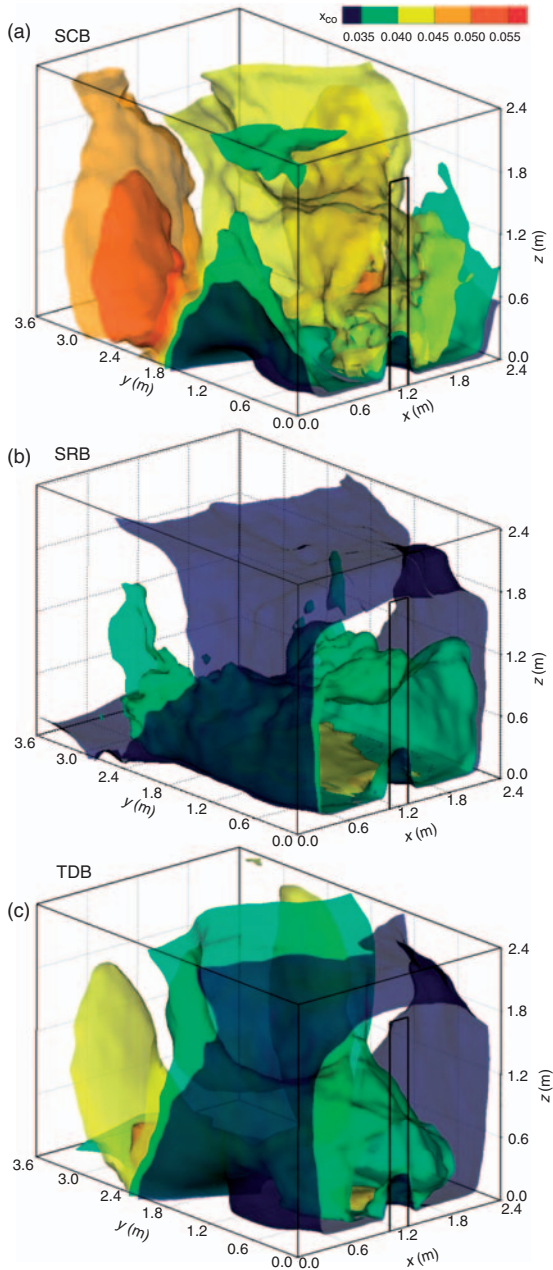


Figure 13. Three-dimensional distributions of mean CO volume fraction inside the compartment.

equivalence ratio difference at the rear circulation region. In the SCB case the fuel concentration is higher in the center region than that in the TDB because all fuel is volatilized at the centered burner as shown in Figure 12. On the other hand, the SRB case yields very different CO distribution compared to the other cases. It is important to note that there is no additional CO at the rear circulating region ( $y \approx 2.4$  m) in the SRB case. The region of maximum CO is concentrated near the front region between the flame and the doorway. From Figure 13, it is obvious that the distribution of fuel in the compartment has an effect on CO concentration. Specifically, the existence/nonexistence of a centered burner leads to a significant difference in the CO at the rear region inside the compartment. It can be also inferred that in the underventilated fire condition, the distance between the fuel and the doorway played a significant role in determining flow dynamics, and the thermal and chemical environment inside the compartment.

## CONCLUSIONS

Experiments were conducted to investigate the effects of fuel distribution on underventilated compartment fires including the global burning characteristics, the thermal and chemical environment, and flow dynamics when fuel location and distribution are changed in the full-scale ISO 9705 room. Detailed comparisons of global parameters, temperature, heat flux, and species concentrations including multi-dimensional fire behavior as a function of fuel placement are presented.

From the experimental results, it was observed that varying the fuel location and distribution does not play an important role in changing the global characteristics of an underventilated fire such as the fuel mass loss rate, HRR, combustion efficiency, global equivalence ratio, and global CO emission outside the compartment. These results are different than what has been observed in overventilated fires [4].

The local thermal and chemical environments were different depending on the fuel location. At the front of the compartment, the thermal and chemical environments are nearly the same regardless of fuel location and distribution. However, variation in fuel placement resulted in significant changes in temperature, total heat flux, CO<sub>2</sub>, and CO distributions at the rear of the compartment. The detailed causes of these phenomena were discussed in terms of the calculated multi-dimensional fire behavior using the numerical simulation. The location of the flame stoichiometric surface was nearly the same for all cases in the front region. In the rear region, it was observed that the change in fuel placement results in a significant change in the flow field. These results are consistent with the

experimental results that the thermal and chemical environments in the rear region change as the fuel placement changed inside the compartment.

The existence-nonexistence of a centered burner brings about a change in the mixture fraction distribution as well as the flow dynamics. A significant difference in CO at the rear region occurs when the fuel is placed at different locations within the compartment. It can be also inferred from these results that the distance between the fuel and the vent plays a significant role in determining flow dynamics, and the thermal and chemical environment within the compartment.

## ACKNOWLEDGMENTS

The authors thank Richard Harris, Kevin McGrattan and Bryan Klein for helpful discussions and Lauren DeLauter, Doris Reinhart, Tony Chakalis, and Kelly Opert for their technical assistance. C.-H. Hwang gratefully acknowledges support from a Korean Research Foundation Grant funded through the Korean Government (MOEHRD) (KRF-2007-357-D00028).

## REFERENCES

1. Novozhilov, V. (2001). Computational Fluid Dynamics Modeling of Compartment Fires, *Progress in Energy and Combustion Science*, **27**: 611–666.
2. Bryner, N.P., Johnsson, E.L. and Pitts, W.M. (1994). Carbon Monoxide Production in Compartment Fires – Reduced-scale Enclosure Test Facility, NISTIR 5568, National Institute of Standards and Technology, Gaithersburg, MD.
3. Yii, E.H., Buchanan, A.H. and Fleischmann, C.M. (2006). Simulating the Effects of Fuel Type and Geometry on Post-flashover Fire Temperatures, *Fire Safety Journal*, **41**: 62–75.
4. Thomas, I.R., Moinuddin, K.A. and Bennetts, I.D. (2007). The Effect of Quantity and Location on Small Enclosure Fires, *Journal of Fire Protection Engineering*, **17**: 85–102.
5. Utiskul, Y., Quintiere, J.G., Rangwala, A.S., Ringwelski, B.A., Wakatsuki, K. and Naruse, T. (2005). Compartment Fire Phenomena Under Limited Ventilation, *Fire Safety Journal*, **40**: 367–390.
6. Lock, A., Bundy, M., Johnsson, E.L., Hamins, A., Ko, G.H., Hwang, C., Fuss, P. and Harris, R. (2008). Experimental Study of the Effects of Fuel Type, Fuel Distribution, and Vent Size on Full-scale Underventilated Compartment Fires in an ISO 9705 Room, NIST Technical Note 1603, National Institute of Standards and Technology, Gaithersburg, MD.
7. Bundy, M., Hamins, A., Johnsson, E.L., Kim, S.C., Ko, G.H. and Lenhert, D. (2007). Measurements of Heat and Combustion Products in Reduced-scale

- Ventilation-limited Compartment Fires, NIST Technical Note 1483, National Institute of Standards and Technology, Gaithersburg, MD.
8. Quintiere, J.G., Rinkinen, W.J. and Jones, W.W. (1981). The Effect of Room Openings on Fire Plume Entrainment, *Combustion Science and Technology*, **26**: 193–201.
  9. Merci, B. and Vandevelde, P. (2007). Experimental Study of Natural Roof Ventilation in Full-scale Enclosure Fire Tests in a Small Compartment, *Fire Safety Journal*, **46**: 523–535.
  10. Pierce, J.B.M. and Moss, J.B. (2007). Smoke Production, Radiation Heat Transfer and Fire Growth in a Liquid-Fuelled Compartment Fire, *Fire Safety Journal*, **42**: 310–320.
  11. Tran, H.C. (1990). Experimental Aspects of Validating a Compartment Wall Fire Model, In: *Proceedings of 5th International Fire Conference, Interflam '90*, London, England, 3–6 September, pp. 13–24.
  12. Snegirev, A.Y., Makhviladze, G.M., Talalov, V.A. and Shamshin, A.V. (2003). Turbulent Diffusion Combustion Under Conditions of Limited Ventilation: Flame Projection Through an Opening, *Combustion Explosion and Shock Waves*, **39**: 1–10.
  13. Bertin, G., Most, J.M. and Coutin, M. (2002). Wall Fire Behavior in an Under-ventilated Room, *Fire Safety Journal*, **37**: 615–630.
  14. Lattimer, B.Y., Hunt, S.P., Wright, M. and Sorathia, U. (2003). Modeling Fire Growth in a Combustible Corner, *Fire Safety Journal*, **38**: 771–796.
  15. Leonard, S., Mulholland, G.W., Puri, R. and Santoro, R.J. (1994). Generation of CO and Smoke During Underventilated Combustion, *Combustion and Flame*, **98**: 20–34.
  16. Pitts, W.M. (1994). Application of Thermodynamic and Detailed Chemical Kinetic Modeling to Understanding Combustion Product Generation in Enclosure Fires, *Fire Safety Journal*, **23**: 271–303.
  17. Pitts, W.M. (1994). The Global Equivalence Ratio Concept and the Prediction of Carbon Monoxide Formation in Enclosure Fires, NIST Monograph 179, National Institute of Standards and Technology, Gaithersburg, MD.
  18. Pitts, W.M. (1995). The Global Equivalence Ratio Concept and the Formation Mechanisms of Carbon Monoxide in Enclosure Fires, *Progress in Energy and Combustion Science*, **21**: 197–237.
  19. McGrattan, K., Hostikka, S., Floyd, J., Baum, H. and Rehm, R. (2008). Fire Dynamics Simulator (Version 5) Technical Reference Guide, NIST SP 1018-5, National Institute of Standards and Technology, Gaithersburg, MD.
  20. Bryant, R.A., Ohlemiller, T.J., Johnsson, E.L., Hamins, A., Grove, B.S., Guthrie, W.F., Maranghides, A. and Mulholland, G.W. (2004). The NIST 3 Megawatt Quantitative Heat Release Rate Facility – Description and Procedure, NISTIR 7052, National Institute of Standards and Technology, Gaithersburg, MD.
  21. Parker, W.J. (1984). Calculations of the Heat Release Rate by Oxygen-consumption for Various Applications, *Journal of Fire Sciences*, **2**: 380–395.
  22. Floyd, J.E., McGrattan, K.B., Hostikka, S. and Baum, H.R. (2003). CFD Fire Simulation using Mixture Fraction Combustion and Finite Volume Radiative Heat Transfer, *Journal of Fire Protection Engineering*, **13**: 11–36.

23. Floyd, J.E. and McGrattan, K.B. (2008). Validation of a CFD Fire Model using Two Step Combustion Chemistry using the NIST Reduced-scale Ventilation-limited Compartment Data, In: *9th International IAFSS Symposium*, Karlsruhe, Germany, 21–26 September.
24. Floyd, J.E. and McGrattan, K.B. (2009). Extending the Mixture Fraction Concept to Address Under-ventilated Fires, *Fire Safety Journal*, **44**: 291–300.
25. Hwang, C.-H., Lock, A., Bundy, M., Johnsson, E. and Ko, G.H. (2009). Studies on Fire Characteristics in Over- and Underventilated Full-scale Compartments, *Journal of Fire Sciences*, doi:10.1177/0734904110363106.
26. Tewarson, A. (1995). Generation of Heat and Chemical Compounds in Fires, *SFPE Handbook of Fire Protection Engineering*, Society of Fire Protection Engineers, Boston, MA.
27. Ceramic fiber blanket K-Lite™. Available at: <http://www.gltproducts.com> (accessed date December 1, 2008)
28. Drysdale, D. (1999). *An Introduction to Fire Dynamics*, John Wiley and Sons, Chichester, UK.
29. Association NFP. (2002). *SFPE Handbook of Fire Protection Engineering*, Society of Fire Protection Engineers, Boston, MA.
30. Hu, Z., Utiskul, Y., Quintiere, J.G. and Trouve, A. (2005). A Comparison between Observed and Simulated Flame Structure in Poorly Ventilated Compartment Fires, In: *Fire Safety Science – Proceedings of the Eight International Symposium*, Beijing, China, 18–23 September, pp. 1193–1204.
31. Kuo, K.K. (1986). *Principles of Combustion*, John Wiley and Sons, New York, USA.
32. Ko, G.H., Hamins, A., Bundy, M., Johnsson, E.L., Kim, S.C. and Lenhart, D.B. (2009). Mixture Fraction Analysis of Combustion Products in the Upper Layer of Reduced-Scale Compartment Fires, *Combustion and Flame*, **156**: 467–476.

## BIOGRAPHIES

### Cheol-Hong Hwang

Cheol-Hong Hwang received PhD (2006) degree in Mechanical Engineering from the Inha University, South Korea. He is currently a guest scientist in the Fire Research Division of the Building and Fire Research Laboratory at the National Institute of Standards and Technology (NIST). His major research interests include combustion and fire dynamics using large eddy simulation, and fundamental phenomena of chemically reacting flows.

### Andrew Lock

Andrew Lock received PhD (2007) degree in Mechanical Engineering from the University of Illinois at Chicago. He is currently a fire

protection engineer in the Fire Research Division of the Building and Fire Research Laboratory at the NIST. His major research interests include fire dynamics, heat transport, fire diagnostics, and electronic fire fighter equipment.

### **Matthew Bundy**

Matthew Bundy received PhD (1998) degree in Mechanical Engineering from Washington State University. He is a mechanical engineer and supervisor of the NIST Large Fire Laboratory. His major research interests include flammability measures for polymeric materials, improved uncertainty of heat release rate measurements in largescale fires, and underventilated compartment fires. Dr. Bundy has authored or coauthored more than 20 scientific publications, which include journal articles, conference papers, and NIST reports. He is a member of the International Association for Fire Safety Science Studies on Fire Characteristics in OVF and UVF Full-scale Compartments 27 (IAFSS), and associate member of the North American Fire Testing Laboratories (NAFTL).

### **Erik Johnsson**

Erik Johnsson received a MS (1991) degree in Mechanical Engineering from Virginia Tech. He is a mechanical engineer in the NIST Fire Research Division. He is responsible for providing engineering design and analysis, and planning and performing a wide range of experiments. His current research interests include carbon monoxide production and prediction, underventilated enclosure fires, and motor coach tire fires. He has had membership in the American Society of Mechanical Engineers, Tau Beta Pi (National Engineering Honor Society), and Pi Tau Sigma (Mechanical Engineering Honor Society).

### **Gwon Hyun Ko**

Gwon Hyun Ko received PhD (2004) degree in Mechanical Engineering from Chung-Ang University, South Korea. He was a guest scientist in Building and Fire Research Laboratory, NIST for 2 years, and now he works as a research professor in Chung-Ang University. His current research interests include water mist suppression, advanced modeling on firemist interaction, and compartment fires.